Design of a *W*-Band TE_{01} Mode Gyrotron Traveling-Wave Amplifier With High Power and Broad-Band Capabilities

David B. McDermott, *Senior Member, IEEE*, Heather H. Song, Yosuke Hirata, Anthony T. Lin, *Senior Member, IEEE*, L. R. Barnett, T. H. Chang, Hsin-Lu Hsu, Peter S. Marandos, J. S. Lee, Kwo Ray Chu, *Fellow, IEEE*, and N. C. Luhmann, Jr.

***Abstract*—A high-power gyrotron traveling-wave amplifier operating in the low-loss TE_{01} mode has been constructed at the University of California, Davis that will be driven by a 100-kV, 5-A electron beam with a pitch angle $(v_\perp/v_z)$ of unity and velocity spread of 5%. The amplifier is predicted by large-signal simulations to generate 140 kW at 92 GHz with 28% efficiency, 50-dB saturated gain and 5% bandwidth. The stability of the amplifier from oscillation has been investigated with linear codes. The threshold current for the absolute instability of the TE_{01} operating mode for the chosen operating parameters is predicted to be 10 A. To suppress the potential gyro–backward-wave oscillator interactions, the interaction circuit with a cutoff frequency of 91 GHz has been loaded with distributed loss so that the single-pass attenuation is 90 dB at 93 GHz. The coaxial input coupler has a predicted and measured coupling of 1 and 2 dB, respectively.**

***Index Terms*—Absolute instability, coaxial input coupler, distributed loss, gyro-backward-wave oscillator (BWO), gyro-traveling–wave tube (TWT) amplifier, gyrotron traveling-wave amplifier, magnetron injection gun (MIG).**

I. INTRODUCTION

WIDE-BAND high average power amplifiers are required in the 92–96-GHz atmospheric window for advanced radar applications [1], [2]. The highest average power from a conventional linear beam slow wave device at 94 GHz is 1 kW and is produced by the CPI 8783 extended interaction amplifier. Further advances are made difficult by the problem of passing an intense electron beam through the extremely narrow circuits needed to support a slow wave at this frequency. Fast wave devices are capable of significantly higher power because their circuits can be significantly larger. Gyrotron devices, which employ a fast wave circuit, generate the highest average power at millimeter wavelengths. A gyroklystron amplifier operating in the low-loss TE_{01} mode has produced an average power of 10 kW at 94 GHz [3]. However, the bandwidth, limited by the Q of the cavities, was less than 1%.

A gyrotron traveling-wave tube amplifier (gyro-TWT) with a nonresonant traveling-wave circuit is capable of much broader bandwidth. Unfortunately, gyro-TWTs have been plagued by instabilities. In one of the first gyro-TWTs [4], oscillation at the cutoff frequency due to an absolute instability [5] forced the device to be strongly detuned, which lowered the gain and bandwidth. The performance was improved by making the walls more resistive (by a factor of $\sim$1000) [6]. Gyro-TWTs can also oscillate as a gyro-backward-wave oscillator (BWO) at the Doppler-shifted cyclotron frequency and its harmonics [7]. It was shown experimentally that this oscillation can also be suppressed by increasing the circuit's attenuation [8]. A *Ka*-Band TE_{11} gyro-TWT, which exhibited both types of oscillation in its initial copper circuit, was stabilized by making the walls of the circuit extremely resistive [9]. The added insertion loss was approximately 100 dB near the cutoff frequency. The resulting high performance amplifier displayed an exceptionally high gain of 70 dB. More recently, a TE_{01} gyro-TWT produced 137 kW in the *Ka*-band by also adding a considerable amount of loss to the circuit [10]. In addition, it must also be noted that a high power gyro-TWT [11] was recently operated at the second-harmonic with an extremely wide bandwidth of 21% by utilizing a novel helically corrugated beat-wave circuit specially designed for stability by substantially altering the coupled dispersion diagram.

This paper describes the design of a high-performance 94-GHz TE_{01} gyro-TWT [12] that applies the same technique of employing distributed wall loss to achieve stability as in Ref. [9]. The TE_{01} mode is employed because its low loss in the output section could potentially allow the amplifier to be operated at high average power and its radial maximum at halfway between the wall and center is ideal for the placement of the electron beam. The amplifier was designed by following the marginal stability design procedure [13], where the electron transverse velocity and beam current are chosen to provide maximum efficiency and gain while keeping the beam current less than the threshold for the absolute instability of the operating mode and the interaction length shorter than the critical length for gyro-BWO oscillation.

Manuscript received December 1, 2001; revised January 26, 2002. This work was supported in part by AFOSR under Grants F49620-99-1-0297 (MURI MVE) and F49620-00-1-0339.

D. B. McDermott, H. H. Song, H.-L. Hsu, P. S. Marandos, J. S. Lee, and N. C. Luhmann, Jr. are with the Department of Applied Science, University of California, Davis, CA 94616 USA (e-mail: dmcdermott@ucdavis.edu).

Y. Hirata was with the Department of Applied Science, University of California, Davis, CA 94616 USA. He is now with the Power and Industrial Systems Research and Development Center, Toshiba Corporation, 210–0882 Kawasaki, Japan.

A. T. Lin is with the Department of Physics, University of California, Los Angeles, CA 90024 USA.

L. R. Barnett, T. H. Chang, and K. R. Chu are with the Department of Physics, National Tsing Hua University, Hsinchu, 300 Taiwan, R.O.C.

Digital Object Identifier 10.1109/TPS.2002.801559

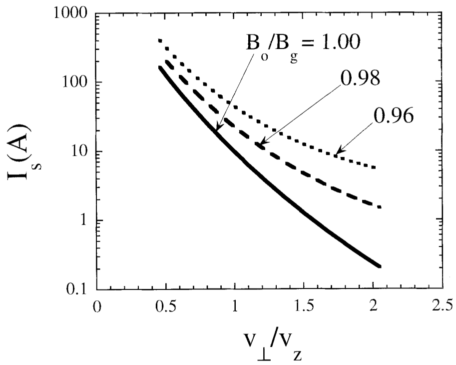

Fig. 1. Dependence of threshold current for absolute instability on velocity ratio $\alpha = v_\perp/v_z$ for three values of magnetic field (100 kV, $r_c/r_w = 0.45$).

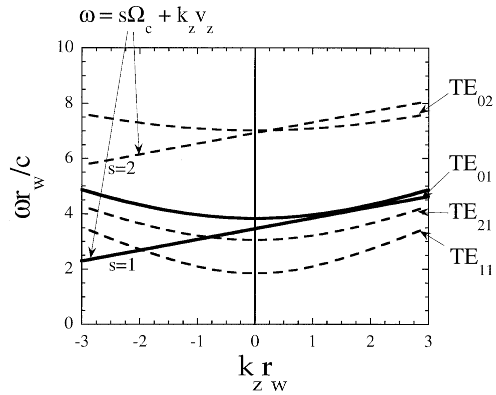

Fig. 2. Dispersion diagram of the operating mode (intersection of unbroken curves) and possible oscillating modes (intersections of broken curves with negative k_z) (100 kV, $v_\perp/v_z = 1.0$).

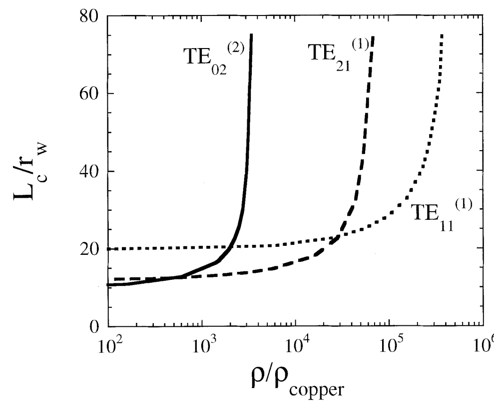

Fig. 3. Dependence on wall resistivity of the critical length for gyro-BWO in the $TE_{11}^{(1)}$, $TE_{21}^{(1)}$, and $TE_{02}^{(2)}$ modes (100 kV, 5 A, $v_\perp/v_z = 1.0, B/B_g = 1.0, r_c/r_w = 0.45$).

The organization of this paper is as follows. The loss required for the amplifier's stability is determined in Section II. Section III describes how the required loss was achieved. The predicted large-signal characteristics of the amplifier are presented in Section IV. Two important ancillary components, the coupler and electron gun, are described in Sections V and VI, respectively. Section VII contains the summary.

II. Stability

The amplifier design was developed by following the marginal stability design procedure [13]. Because a large axial velocity is beneficial for stability and wide bandwidth, the operating voltage of a high power gyro-TWT should be as high as practical. A voltage of 100 kV was chosen. To reduce the interception of electrons by the wall, the guiding center of the beam is 45% of the wall radius, which is slightly inside of the mode maximum. Small-signal codes have been employed to investigate the stability of the amplifier. First, the amplifier must remain stable from the absolute instability of the operating mode [5], which occurs when the gain is sufficiently high that the bandwidth extends to the cutoff frequency [14]. At this point, a wave at cutoff will become unstable and a backward wave will start to grow. The threshold electron beam current for this from saddle-point theory [5], [15] is shown in Fig. 1 for a 100-kV beam whose guiding center radius, r_c, is 45% of the wall radius. Since the TE_{01} mode is predicted to oscillate at 10 A for our planned parameters (100 kV, $v_\perp/v_z = 1.0, B/B_g = 0.995$) in a lossless circuit and loss will add further stability, there is a comfortable safety margin for our planned beam current of 5 A.

The dispersion diagram for the amplifier is shown in Fig. 2. To yield strong amplification over the broadest bandwidth, the cyclotron resonance line nearly grazes the TE_{01} mode. To enhance the efficiency, the magnetic field is slightly detuned ($B/B_g = 0.995$, where B_g is the grazing magnetic field). It is evident there are several potential gyro-BWO modes [7], [16] at the fundamental cyclotron frequency and at the harmonics. The short interaction length needed to stabilize these modes would yield insufficient gain to even overcome the launching loss. However, a recent gyro-TWT experiment [9] has found that loss can stabilize gyro-BWO modes. The critical length for the start of gyro-BWO oscillation in the amplifier with loss and an ideal beam is shown in Fig. 3. Generally, modes that are excited near their cutoff, where the wave impedance is highest, have the lowest start-oscillation length. However, wall loss is more effective close to the cutoff. The $TE_{02}^{(2)}$ mode (the superscript refers to the harmonic number) is closest to cutoff and seen to be most sensitive to wall loss. The $TE_{11}^{(1)}$ mode is least sensitive, but it is anticipated that it will be stabilized by the beam's velocity spread. For a wall resistivity of $70\ 000\rho_{\mathrm{Cu}}$, where ρ_{Cu} is the resistivity of ideal copper ($\rho_{\mathrm{Cu}} = 1.72 \times 10^{-6}\ \Omega\cdot$ cm), the $TE_{21}^{(1)}$ mode is stable for an interaction length of 15 cm.

III. Loss

To produce the required attenuation, the wall of the interaction waveguide was coated with Aquadag, a resistive carbon colloid often used to discharge electron buildup on CRT screens. Aquadag had also been used in the ultrahigh gain TE_{11} gyro-TWT at National Tsing Hua University [9]. Acheson, the manufacturer, reports that Aquadag's resistivity usually falls in the range of $(36\ 000–80\ 000)\rho_{\mathrm{Cu}}$, an extent that includes our desired value. The value reported in Ref. [9] was $36\ 000\rho_{\mathrm{Cu}}$. The actual value depends on the preparation and application method.

There was some concern because the material can alter the cutoff frequency due to its finite thickness. Therefore, the high-

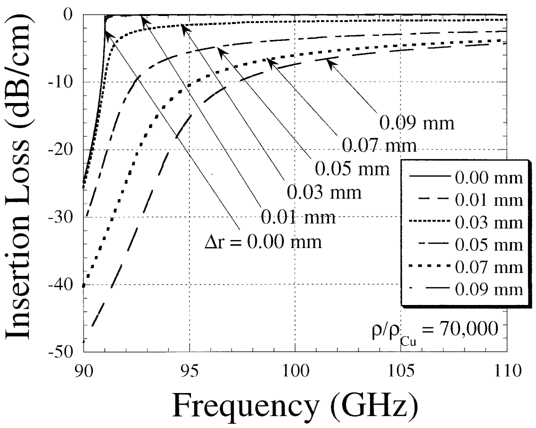

Fig. 4. Dependence on frequency of insertion loss for TE_{01} waves through circuit loaded with a semiconductor liner for several values of thickness ($r_w = 2.01$ cm, $\rho = 70\ 000\rho_{Cu}$). The loss for $\Delta r = 0.01$ mm is nearly indistinguishable from the unloaded case.

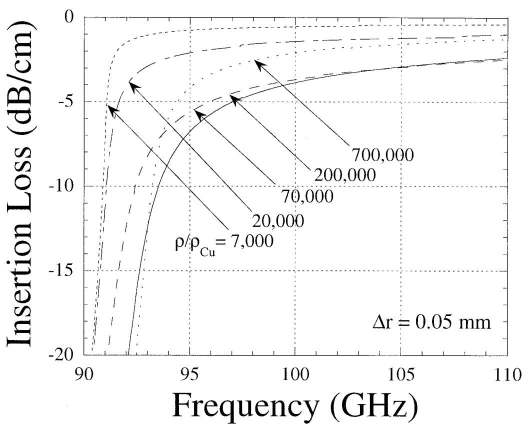

Fig. 5. Dependence on frequency of insertion loss for TE_{01} waves through circuit loaded with a semiconductor liner for several values of resistivity ($r_w = 2.01$ cm, $\Delta r = 0.05$ mm).

frequency structure simulator (HFSS) [17] was employed to determine the optimum thickness and resistance of the lossy material. HFSS models the loss layer as a semiconductor. It was found, however, that the attenuation is not dependent on the value of the dielectric constant. Fig. 4 shows that the loss increases with the material's thickness, but it is unproductive to make the thickness greater than the skin depth. The primary effect of making it any thicker is to alter the effective cutoff frequency. For a resistivity of $70\ 000\rho_{Cu}$, the skin depth at 94 GHz is 0.057 mm. Since it is desired that the loss layer not alter the cutoff frequency by more that a few percent, the thickness should not be greater than a few percent of the wall radius. Fig. 5 shows that for a thickness of 0.05 mm, the highest attenuation occurs for a resistivity in the range of $70\ 000\rho_{Cu}$–$200\ 000\rho_{Cu}$. If the resistivity is any greater, then the loss is reduced because the thickness is significantly less than a skin depth, as is seen to occur for $\rho = 700\ 000\rho_{Cu}$.

The desired effective wall resistivity of $\rho/\rho_{cu} = 70\ 000$ was achieved by coating the first 12 cm of the interaction circuit with sixteen layers of Aquadag. Through trial and error, by varying the dilution ratio with water, the precise value needed to suppress the $TE_{21}^{(1)}$ gyro-BWO mode was attained. Fig. 6 compares

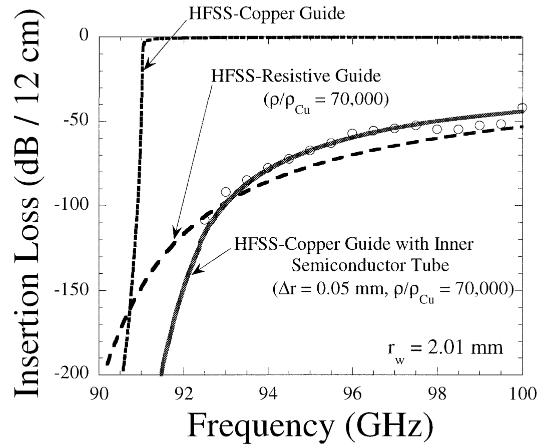

Fig. 6. Dependence on frequency of TE_{01} mode's insertion loss through 12-cm-length circuit from HFSS simulation (curves) and measurement (symbols). The broken curve shows the HFSS predictions for a semiconductor tube with a resistivity 70 000 times copper within copper waveguide. The unbroken curves are the predictions for a metallic waveguide with the resistivity of copper and 70 000 times copper.

the measurements of our final Aquadag-loaded circuit to our HFSS simulation of several appropriate cases. It is seen that the measurements of the lossy circuit agree well with the HFSS simulation of transmission through 12 cm of copper waveguide loaded with a 0.05-mm thickness semiconductor tube with a resistivity of 70 000 times copper. Furthermore, both agree with the HFSS simulation of transmission through 12 cm of unloaded metallic waveguide, whose resistivity is 70 000 times copper, which is the case that had been found to suppress the $TE_{21}^{(1)}$ gyro-BWO (Fig. 3). Specifically, the loss was measured to be 90 dB at 93 GHz, as desired.

IV. Large-Signal Characteristics

Our self-consistent nonlinear particle-tracing code [18], [19] was modified so that it includes distributed wall loss and then employed to evaluate the large-signal characteristics of the amplifier. The code also includes reflections from the finite-mismatch of the input and output couplers and the loss taper. The amplifier parameters are given in Table I. So that the wave is not damped in the high power region, there is no loss added to the final 2.5 cm of the circuit and the loss in the preceding 1 cm is linearly tapered. When it is equipped with the proper collector and cooling, this would allow the device to operate continuously at an average power of 140 kW with only 50-W/cm^2 peak wall loading, well below the typical upper limit of 1 kW/cm^2 for continuous wave (CW) gyrotrons [20], albeit with all metal surfaces. The power handling capablity of Aquadag is not known for sure, but it is likely that it can handle this load since it is regularly baked at 200°C as part of its normal curing process. Furthermore, Aquadag combined with iron has been successfully used in the severs of high average power coupled-cavity TWTs. Employing a fairly thick annulus of lossy ceramic so that it corresponds to the outer lobe of the TE_{02} mode as employed in [10] is another method for distributing the required loss and handling the high power. Fig. 7 shows the axial profile of the convective power growth in the amplifier. There is an inflection point near

TABLE I
DESIGN PARAMETERS OF THE HEAVILY LOADED TE_{01} GYRO-TWT AMPLIFIER

Voltage	-100 kV
Current	5 A
$\alpha = v_\perp/v_z$	1.0
$\Delta v_z/v_z$	5%
Magnetic Field, B_o	35.6 kG
B_o / B_g	0.995
Cutoff Frequency	91.0 GHz
Lossy Wall Resistivity	70,000 ρ_{Cu}
Guiding Center Radius, r_c	0.45 r_w
Circuit Radius, r_w	0.201 cm
Lossy Circuit Length	11.0 cm
Loss Taper Length	1.0 cm
Copper Circuit Length	2.5 cm
Total Circuit Length	14.5 cm

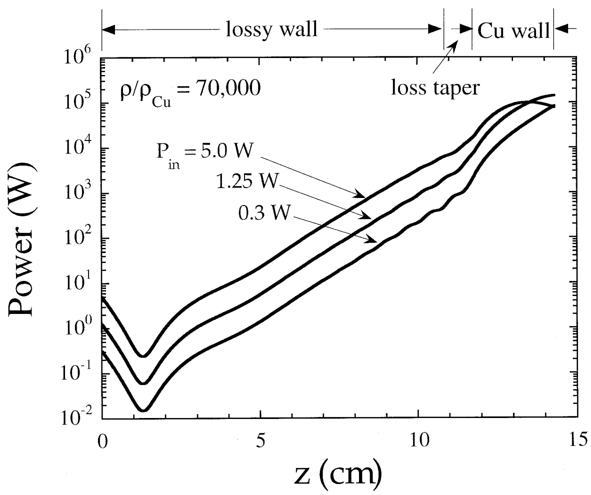

Fig. 7. Axial power growth of 92.25-GHz wave in the loaded TE_{01} circuit for three values of input power (Table I).

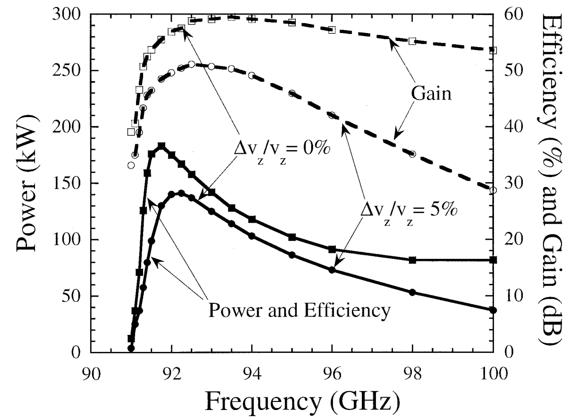

Fig. 8. Saturated bandwidth of the output power (unbroken line), efficiency (unbroken line), and gain (broken line) for an axial velocity spread of 0% and 5% (Table I).

(a)

(b)

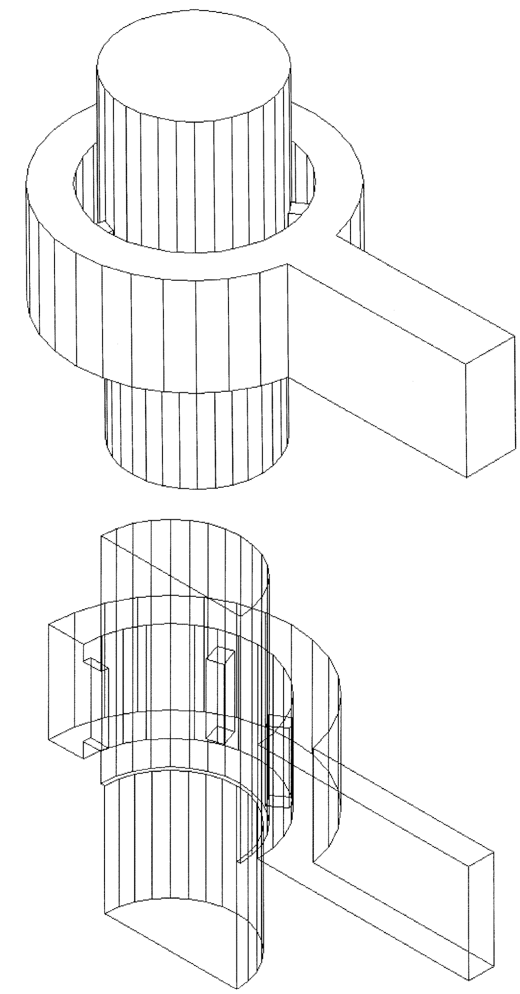

Fig. 9. Schematic of the TE_{01} coaxial-filter input coupler. (a) With hidden line. (b) Cut through the center.

the beginning of the unloaded region where the growth rate increases. Theory indicates that a gyro-TWTs gain will decrease by one third of the added loss [21]. Although the loss reduces the growth rate, it was found to have little effect on the efficiency. For an axial velocity spread of $\Delta v_z/v_z = 5\%$, the predicted peak power is 140 kW with an efficiency of 28% and a saturated bandwidth of 5%, as shown in Fig. 8. The large-signal gain is 50 dB, even though the circuit has 90 dB of loss at the frequency of 93 GHz.

V. TE_{01} COUPLER

A coaxial input coupler has been designed with HFSS with a 1-dB insertion loss over a bandwidth of 3%. It is similar to the azimuthal phase velocity coupler used in the University of California, Los Angeles $TE_{61}^{(6)}$ gyro-TWT [22] and the coupler in the high average power 94 GHz TE_{01} gyroklystron [3]. As shown in Fig. 9, the input signal is injected from conventional rectangular waveguide into the coaxial TE_{51} mode of a coaxial cavity and then into the desired TE_{01} mode of the cylindrical interaction waveguide within the inner coax through five slots in

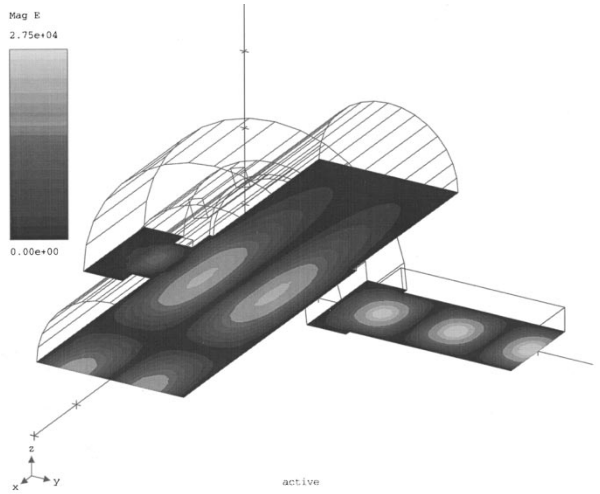

(a)

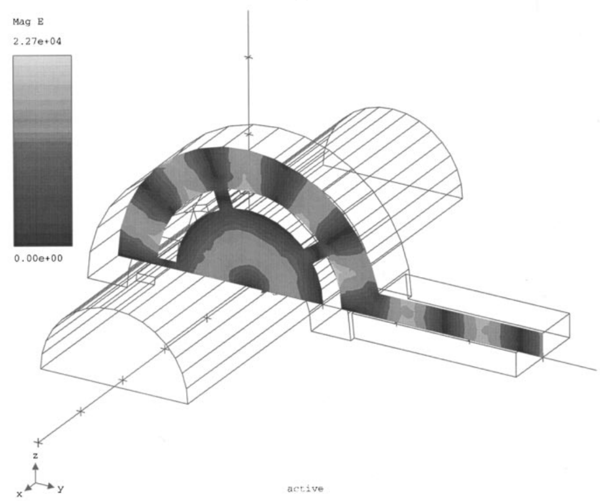

(b)

Fig. 10. Intensity of electromagnetic waves in the TE_{01} coaxial-filter input coupler from HFSS. (a) An axial view cut through the axis. (b) A cross-sectional view through the coaxial cavity.

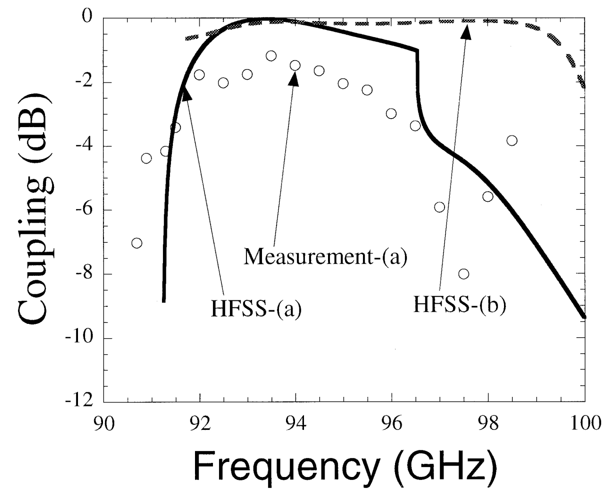

Fig. 11. Bandwidth of the insertion loss through the TE_{01} coaxial-filter input coupler [Table II(a)] from measurement and HFSS and for a future coupler [Table II(b)] from HFSS.

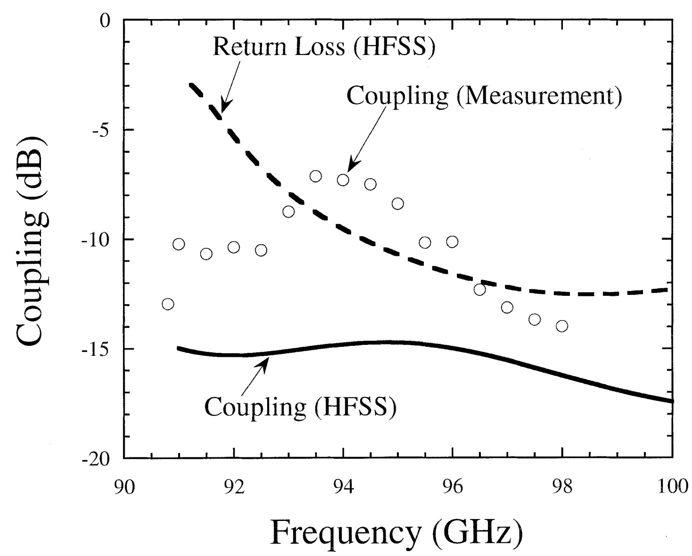

Fig. 12. Bandwidth of the insertion loss through the TE_{01} coaxial-filter output coupler from measurement and HFSS [Table II(c)].

the wall. The design parameters are given in Table II(a). Fig. 10 shows the input and coupled waves from HFSS in two planes. In Fig. 10(a), the effect of the upsteam short is evident. The short is merely a radial discontinuity one quarter wavelength upstream in the drift tube to cutoff and reflect the wave. Further upstream is an annular load to terminate the circuit. In this way, the coupler is a good match for all modes. From the symmetry of the wave pattern in Fig. 10(b), it is clear that a TE_{51} wave in the coaxial cavity is coupling to a TE_{01} wave in the inner waveguide.

Fig. 11 compares the measured coupling with the HFSS predictions. Whereas HFSS predicts greater than -1-dB coupling over a 3% bandwidth, the input coupler actually exhibits a minimum of -2-dB coupling over this bandwidth. The input coupler's performance is limited by the 96.5-GHz cutoff of the upstream short. The discontinuity in the bandwidth can be shifted to higher frequency by reducing the inner diameter of the short. Fig. 11 also shows the wider bandwidth predicted for the design in Table II(b) with a reduced diameter short and where the resonant frequency of the coaxial cavity has been increased to 95 from 94 GHz. Although the modified coupler's predicted bandwidth of 7% is much more suitable for the amplifier's predicted bandwidth of 5% (Fig. 8), the initial tests will employ the former design, since good transmission of the electron beam is a more important concern in the early stages.

An output coupler has been fabricated with the parameters in Table II(c) to monitor the output power. To avoid high power breakdown in the rectangular waveguide, it was designed for a coupling of 10–20 dB. It has the same coaxial geometry, but is a four-port coupler. The TE_{51} coaxial cavity connects to a second identical rectangular waveguide positioned 180° in azimuth from the first. The fourth port is terminated to yield a good match. Fig. 12 compares the measured coupling of the output coupler with the HFSS predictions. The output coupler exhibits greater than -10 dB coupling over a 5% bandwidth. The measured coupling is 5–10 dB higher than the HFSS predictions. This may be due to the fact that the coupling is very sensitive to the length of the coupling slots and there is some uncertainty as to their exact length. However, this poses no problem for the

TABLE II
DESIGN PARAMETERS OF THE TE_{01} COUPLERS: (a) INPUT COUPLER, (b) FUTURE INPUT COUPLER, AND (c) OUTPUT COUPLER

	(a)	(b)	(c)
Coax cavity outer radius, r_{out}	3.586 mm	3.586 mm	3.586 mm
Coax cavity inner radius, r_{in}	2.51 mm	2.61 mm	2.51 mm
Coax cavity length, L_{cav}	2.87 mm	2.70 mm	2.87 mm
Circular waveguide radius, r_w	2.01 mm	2.01 mm	2.01 mm
Circular short radius, r_w	1.90 mm	1.80 mm	--
Dimensions of rectangular input guide	2.87 mm × 1.435 mm	2.70 mm × 1.35 mm	2.87 mm × 1.435 mm
Dimensions of coupling slots (five)	2.0 mm × 0.3 mm	2.7 mm × 0.4 mm	1.3 mm × 0.3 mm
Axial position of cavity start	0.0 mm	0.0 mm	0.0 mm
Axial position of coupling slot center, z_c	1.0 mm	1.35 mm	0.6 mm
Axial position of short, z_s	-0.53 mm	-0.27 mm	--
Azimuthal position of rectangular waveguide	0°	0°	0°, 180°
Azimuthal position of five slots	36°, 108°, 180°, 252°, 324°	36°, 108°, 180°, 252°, 324°	36°, 108°, 180°, 252°, 324°

TABLE III
DESIGN PARAMETERS OF THE SINGLE-ANODE MIG

Cathode Voltage	-100 kV
Emitted Current	5 A
Cathode Angle	74°
Electric Field	70 kV
Magnetic Compression	32
Cathode Radius	5.1 mm
Emitting Strip Length	1.9 mm
Guiding Center Radius (Circuit)	0.9 mm
Guiding Center Spread (Circuit)	10%
$\alpha = v_\perp/v_z$ (Circuit)	1.0
Axial Velocity Spread (Circuit)	5%
Cathode Loading	9 A/cm^2
J_{emis}/J_L	0.3

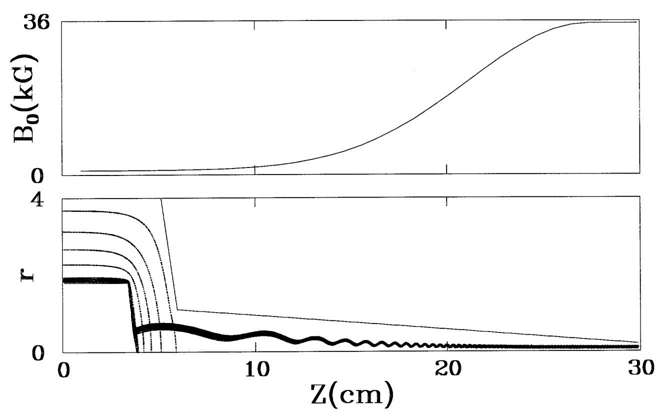

Fig. 13. Electron trajectories and electrostatic contours for the MIG from FINELGUN simulation and the magnetic field profile.

experiment, since this coupler is just a monitor and the coupling has been measured and calibrated for all frequencies of interest. In the initial hot tests, most of the generated TE_{01} wave will be absorbed in a downstream annular load.

VI. ELECTRON GUN

To achieve the wide bandwidth predicted by theory (Fig. 8), it is crucial that the electron beam has a low velocity spread. A single-anode magnetron injection gun (MIG) electron gun has been designed using the variable mesh code FINELGUN [24]. The initial values were found by solving the set of equations for the constants of motion given in Ref. [23]. For a MIG gun with a sufficiently large cathode angle, it is no longer necessary to keep the gap between the inner and outer electrodes larger than twice the Larmor radius. For large angles, the geometry becomes less coaxial and more planar. The design parameters of the MIG are listed in Table III. The MIG has a very large cathode angle of 74° and is shown in Fig. 13. The 100-kV, 5-A electron beam with $v_\perp/v_z = 1.0$ has a predicted axial velocity spread of 5%. The MIG gun has been fabricated. It is a modification of the NTHU MIG design [25] and employs a dispenser cathode manufactured by Spectramat. The edges of the emitting strip have

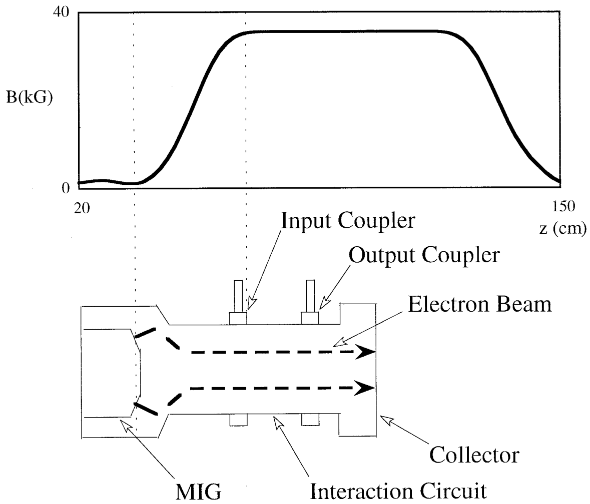

Fig. 14. Schematic of the TE_{01} gyro-TWT amplifier and the planned axial magnetic field profile.

been coated with Molybdenum to suppress edge emission. The MIG has been activated and the *I–V* characteristics have been measured. The gun displays a space-charge-limited perveance of 1.3 μP at 1 kV, but will be temperature limited to a perveance of 0.16 μP at the operating value of 100 kV.

VII. Summary

The design of a high-power gyro-TWT amplifier that is predicted by a large-signal simulation code to generate 140 kW at 92 GHz with 28% efficiency, 50-dB saturated gain and 5% bandwidth has been presented. It will operate in the low-loss TE_{01} mode and be driven by a 100-kV, 5-A, MIG electron beam with $v_\perp/v_z = 1$ and $\Delta v_z/v_z = 5\%$. When fitted with cooling and an appropriate waveguide collector, the device is potentially capable of cw operation. The stability of the amplifier from oscillation has been checked with linear codes. The operating beam current is less than the threshold value for absolute instability. To suppress the potential gyro–BWO interactions, the interaction circuit has been loaded with lossy Aquadag. The required insertion loss for the circuit at 93 GHz from theory is 90 dB, which was achieved. A coaxial input coupler with 3% bandwidth was designed with 1-dB coupling and measured with 2-dB coupling. In addition, another coaxial input coupler was designed with 0.5-dB coupling over a 7% bandwidth.

A wire-wound helical waveguide [26]–[28] was considered as the interaction circuit for this TE_{01} gyro-TWT. This waveguide takes advantage of the unique purely azimuthal nature of the TE_{0n} wall currents and attenuates TE_{mn} waves with $m \neq 0$, but transmits TE_{0n} waves with little loss. It is an ideal TE_{0n} mode selective circuit. This will be the subject of future investigations.

The initial tests have begun and are being performed in a 50-kG superconducting magnet. The axial profile of the magnetic field is shown in Fig. 14 together with a schematic of the gyro-TWT amplifier. The solenoid contains four independent compensated coils. The two interaction coils produce a very weak magnetic field in the gun region and the two gun coils produce almost zero field in the interaction region. Both regions have solenoidal and gradient coils. By positioning the emitter at the null of the gun gradient coil, both the amplitude and gradient of the axial magnetic field at the cathode can be independently adjusted. A 100-W coupled-cavity TWT amplifier will drive the gyro-TWT into saturation and a 1-kW EIO is available as a back-up source.

References

[1] L. A. Hoffman, K. H. Hurlbut, D. E. Kind, and H. J. Wintroub, "A 94-GHz radar for space object identification," *IEEE Trans. Microwave Theory Tech.*, vol. MTT-17, pp. 1145–1149, 1969.
[2] W. M. Manheimer, G. Mesyats, and M. I. Petelin, "Applications of high power microwave sources to enhanced radar systems," in *Applications of High Power Microwaves*, A. V. Gaponov-Grekhov and V. L. Granatstein, Eds. Boston, MA: Artech House, 1994, pp. 169–207.
[3] M. Blank *et al.*, "Demonstration of a 10 kW average power 94 GHz gyroklystron amplifier," *Phys. Plasmas*, vol. 6, pp. 4405–4409, 1999.
[4] L. R. Barnett, K. R. Chu, J. M. Baird, V. L. Granatstein, and A. T. Drobot, "Gain, saturation, and bandwidth measurements of the NRL gyrotron traveling-wave amplifier," in *IEEE IEDM Tech. Dig.*, 1979, pp. 164–167.
[5] Y. Y. Lau, K. R. Chu, L. R. Barnett, and V. L. Granatstein, "Gyrotron travelling wave amplifier: I. Analysis of oscillations," *Int. J. Infrared Millimeter Waves*, vol. 2, pp. 373–393, 1981.
[6] L. R. Barnett, J. M. Baird, Y. Y. Lau, K. R. Chu, and V. L. Granatstein, "A high gain single stage gyrotron traveling-wave amplifier," in *IEEE IEDM Tech. Dig.*, 1980, pp. 314–317.
[7] K. R. Chu, L. R. Barnett, W. K. Lau, L. H. Chang, and C. S. Kou, "Recent developments in millimeter wave gyro-TWT research at NTHU," in *IEEE IEDM Tech. Dig.*, 1990, pp. 699–702.
[8] K. R. Chu, L. R. Barnett, H. Y. Chen, S. H. Chen, Ch. Wang, Y. S. Yeh, Y. C. Tsai, T. T. Yang, and T. Y. Dawn, "Stabilization of absolute instabilities in the gyrotron traveling-wave amplifier," *Phys. Rev. Lett.*, vol. 74, pp. 1103–1106, 1995.
[9] K. R. Chu, H. Y. Chen, C. L. Hung, T. H. Chang, L. R. Barnett, S. H. Chen, and T. T. Yang, "Ultrahigh gain gyrotron traveling-wave amplifier," *Phys. Rev. Lett.*, vol. 81, pp. 4760–4763, 1998.
[10] M. Garven, J. P. Calame, B. G. Danly, K. T. Nguyen, D. E. Pershing, B. Levush, F. N. Wood, and D. E. Pershing, "A gyrotron-traveling-wave tube amplifier experiment with a ceramic loaded interaction region," *Trans. Plasma Sci.*, vol. 30, pp. 886–894, June 2002.
[11] V. L. Bratman, A. W. Cross, G. G. Denisov, W. He, A. D. R. Phelps, K. Ronald, S. V. Samsonov, C. G. Whyte, and A. R. Young, "High-gain wide-band gyrotron traveling-wave amplifier with a helically corrugated waveguide," *Phys. Rev. Lett.*, vol. 84, pp. 2746–2749, 2000.
[12] Y. Hirata, D. B. McDermott, A. T. Lin, T. H. Chang, K. R. Chu, and N. C. Luhmann Jr., "W-band TE_{01} gyro-TWT with heavy wall loss," in *Dig. 25th Int. Conf. Infrared and Millimeter Waves*, Beijing, China, 2000, pp. 179–180.
[13] A. T. Lin, K. R. Chu, C. C. Lin, C. S. Kou, D. B. McDermott, and N. C. Luhmann Jr., "Marginal stability design criterion for gyro-TWTs and comparison of fundamental with second harmonic operation," *Int. J. Electron.*, vol. 72, pp. 873–885, 1992.
[14] K. R. Chu and A. T. Lin, "Gain and bandwidth of the gyro-TWT and CARM amplifier," *IEEE Trans. Plasma Sci.*, vol. 16, pp. 90–104, Apr. 1988.
[15] R. J. Briggs, *Electron Stream Interaction with Plasma*. Cambridge, MA: MIT Press, 1964, ch. 2.
[16] S. Y. Park, V. L. Granatstein, and R. K. Parker, "A linear theory and design study for a gyrotron backward wave oscillator," *Int. J. Electron.*, vol. 57, pp. 1109–1123, 1984.
[17] "Hewlett Packard 85 180A High-frequency structure simulator," Tech. Rep. HP, Part no. 85180-90037, May 1992.
[18] Q. S. Wang, C. S. Kou, D. B. McDermott, A. T. Lin, K. R. Chu, and N. C. Luhmann Jr., "High-power harmonic gyro-TWT—Part II: Nonlinear theory and design," *IEEE Trans. Plasma Sci.*, vol. 20, pp. 163–169, June 1992.
[19] K. R. Chu, H. Y. Chen, C. L. Hung, T. H. Chang, L. R. Barnett, S. H. Chen, T. T. Yang, and D. Dialetis, "Theory and experiment of ultrahigh gain gyrotron traveling-wave amplifier," *IEEE Trans. Plasma. Sci.*, vol. 27, pp. 391–404, 1999.
[20] M. V. Kartikeyan, E. Borie, and M. K. Thumm, "Possible operation of a 1.5–2-MW, CW conventional cavity gyrotron at 140 GHz," *IEEE Trans. Plasma Sci.*, vol. 28, pp. 645–651, June 2000.

[21] Y. Y. Lau, K. R. Chu, L. Barnett, and V. L. Granatstein, "Gyrotron travelling wave amplifier: II. Effects of velocity spread and wall resistivity," *Int. J. Infrared Millimeter Waves*, vol. 2, pp. 395–413, 1981.
[22] D. S. Furuno, D. B. McDermott, C. S. Kou, N. C. Luhmann Jr., and P. Vitello, "Theoretical and experimental investigation of a high-harmonic gyro-traveling-wave-tube amplifier," *Phys. Rev. Lett.*, vol. 62, pp. 1314–1317, 1989.
[23] J. M. Baird and W. Lawson, "Magnetron injection gun (MIG) design for gyrotron application," *Int. J. Electron.*, vol. 61, pp. 953–967, 1986.
[24] M. Caplan and C. Thorington, "Improved computer modeling of magnetron injection gun for gyrotrons," *Int. J. Electron.*, vol. 51, pp. 415–426, 1981.
[25] Ch. Wang, Y. S. Yeh, T. T. Yang, H. Y. Chen, S. H. Chen, Y. C. Tsai, L. R. Barnett, and K. R. Chu, "A mechanically tunable magnetron injection gun," *Rev. Sci. Instrum.*, vol. 68, pp. 3031–3035, 1997.
[26] S. P. Morgan and J. A. Young, "Helix waveguide," *Bell. Syst. Tech. J.*, vol. 35, pp. 1347–1384, 1956.
[27] W. D. Warters, "The effect of mode filters on the transmission characteristics of circular electric waves in a circular waveguide," *Bell. Syst. Tech. J.*, vol. 37, pp. 657–677, 1958.
[28] *Millimeter Products Incorporated (MPI) Sales Catalogue*. MPIs #340 product line continues TRGs #340 former product line.

David B. McDermott (M'83–SM'92) received the B.S. degree in physics from University of California, Davis in 1976, and the M.A. and Ph.D. degrees in applied physics from Columbia University, New York, in 1977 and 1979, respectively.

He has remained actively involved in the field of electron/wave interaction since he began his graduate research in 1977 to develop a high power, submillimeter-wave free electron laser. After a Postdoctoral position at Columbia University, he joined the Department of Electrical Engineering in 1981. His research at the University of California, Los Angeles (UCLA), contributed to the advancement of millimeter-wave, high-harmonic gyrotron oscillators, and amplifiers. In 1994, he transferred to the Department of Applied Science at University of California, Davis, as a Research Engineer to manage a program developing high power fast-wave sources. He is particularly interested in the interplay between harmonic interaction and symmetry and has also contributed to the evolution of microwave and quasioptical components, including broad-band, overmoded couplers, mode converters, and low loss transmission lines. He is the author of 70 scientific papers and more than 300 scientific presentations at conferences in the areas of microwave generation and electromagnetic circuits.

Dr. McDermott is a Member of APS.

Heather H. Song received the B.S. and M.S. degrees in physics from Ewha Woman's University, Seoul Korea, in 1993 and 1995, respectively. She is currently working toward the Ph.D. degree in the Department of Applied Science, University of California, Davis.

Her current research includes the design, construction, and characterization of high-power *W*-band microwave vacuum devices-gyrotron traveling-wave amplifiers and gyrotron backward wave oscillators. She is also interested in high-power microwave harmonic devices for communications.

Yosuke Hirata was born in Osaka, Japan, on March 5, 1965.

He joined the Research and Development Center, Toshiba Corporation, Kawasaki, Japan, in 1989, where he was engaged in the study of high-power gyrotrons and high-power millimeter-wave transmission. He was on leave at University of California, Davis, from 1998 to 2000, where he was involved in the development of *W*-band gyro-TWTs. He is now with the Power and Industrial Systems Research and Development Center, Toshiba Corporation.

Anthony T. Lin (SM'95) received the Ph.D. degree in electrical engineering from the University of Michigan (UOM), Ann Arbor, in 1970.

Following his graduate work, he was with Space Plasma Laboratory (UOM) for two years and carried out research in the area of beam-plasma interaction in space plasmas. From 1972 to 1973, he was with the Princeton Plasma Laboratory, Princeton, NJ, where he performed particle simulations on the concept of plasma lasers and free electron lasers. In 1973, he joined the University of California at Los Angeles (UCLA), where he has since been developing a variety of new PIC codes and performing research on nonlinear phenomena in plasma physics such as parametric instabilities and anomalous plasma transport. Since the early 1980s, he has extended the particle simulation techniques in plasma physics to the area of microwave generation from relativistic electron beams and developed a number of multitransverse mode PIC codes to study several microwave devices. Using computer simulations, his effort is directed at elucidating basic physics issues in these devices, as well as exploring novel schemes of generating radiation and enhancing their performance. He has authored more than 130 refereed publications.

Dr. Lin was elected Fellow of the American Physical Society.

L. R. Barnett, photograph and biography not available at the time of publication.

T. H. Chang, photograph and biography not available at the time of publication.

Hsin-Lu Hsu received the B.S. and M.S. degrees in physics from National Tsing Hua University, Hsinchu, Taiwan, R.O.C., in 1999 and 2001, respectively. She is currently working toward the Ph.D. degree in the Department of Applied Science, University of California, Davis.

In her Master's thesis, she optimized the coupler for the TE_{01} *W*-band Gyro-TWT. She is currently working on refining the MIG for this experiment.

Peter S. Marandos received the B.S. degree in physics from the California State University, Sacramento, in 1998 and is currently working on the Masters degree in the Department of Applied Science, University of California, Davis.

He is involved in the design, construction, and characterization of *W*-band gyrotron amplifiers and oscillators.

Mr. Marandos is a Member of the American Vacuum Society (AVS) and the International Society for Optical Engineering (SPIE).

J. S. Lee, photograph and biography not available at time of publication.

Kwo Ray Chu (SM'82–F'97) received the B.S. degree in physics from National Taiwan University, Taipei, Taiwan, R.O.C., in 1965, the M.S. degree in physics from the University of Massachusetts, Amherst, in 1968, and the Ph.D. degree in applied physics from Cornell University, Ithaca, NY, in 1972.

From 1973 to 1983, he served in the High Power Electromagnetic Radiation Branch, U.S. Naval Research Laboratory (NRL), Washington, DC, where he headed the Advanced Concepts Section from 1980 to 1983, conducting research on relativistic electronics with emphasis on coherent electromagnetic radiation generation, while concurrently serving as Adjunct Associate Professor in the Department of Applied Sciences, Yale University, New Haven, CT. Since September 1983, he has been a Professor of Physics with National Tsing Hua University, Hsinchu, Taiwan. He is the author or coauthor of over 100 scientific papers, three book chapters, and 11 patents. His research interests include plasma physics, electromagnetics, and relativistic electronics.

Dr. Chu received the Publication Award, the Invention Award, and the Special Achievement Award from the U.S. Naval Research Laboratory, and the Outstanding Research Achievement Award from the National Science Council, Taiwan. He was elected Fellow of the American Physical Society in 1983. In 1997, he was awarded the title of National Chair by the Ministry of Education, Taiwan. He was the recipient of the 2001 IEEE Plasma Science and Application Award and the 2001 K. J. Button Medal and Prize of the British Institute of Physics.

N. C. Luhmann, Jr., photograph and biography not available at the time of publication.